ChemComm

Check for updates

Chemical exchange of labile protons by deuterium enables selective detection of pharmaceuticals in solid formulations†

Claire Welton,‡[a] Parth Raval,‡[a] Julien Trébosc[b] and G. N. Manjunatha Reddy ⓘD ⋆[a]

Chemically assisted swapping of labile protons by deuterons is presented for amino acids, polysaccharides, pharmaceutical compounds, and their solid formulations. Solid-state packing interactions in these compounds are elucidated by ^1H–^2H isotope correlation NMR spectroscopy (iCOSY). A minuscule concentration of dopamine, 5 wt% or ~100 μg, in a solid formulation can be detected by ^2H NMR at 28.2 T (^1H, 1200 MHz) in under a minute.

Site-selective deuteration of small molecules has emerged as an indispensable tool in a variety of research areas such as drug development, structural biology, kinetic isotopic effects, and probing biochemical/enzymatic reactions.[1–6] In particular, deuterated active pharmaceutical ingredients (d-APIs or deuterium isotopologues) have received significant attention owing to their unique physicochemical properties. The d-APIs tend to significantly alter pharmacokinetic properties by retarding the metabolism *in vivo*, which can extend the lifetime of therapeutics, enabling lower dosing than the conventional APIs to achieve the same physiological activity, selectivity and biochemical potency.[3–6] In addition, deuterated amino acids and nucleotides have garnered interest in chemical biology for probing enzymatic/metabolic pathways.[7,8]

Deuterium (^2H) isotopic labelling can be achieved by *de-novo* synthesis of small molecules using heterogeneous catalysis or enzymatic reactions.[9–12] Nanostructured iron catalysts have been employed to selectively deuterate CH sites in (hetero)arenes and heterocycles such as anilines, phenols, and indoles.[9,13] Dual-protein catalysis has been shown to deuterate C_α and C_β sites in amino acids.[14] Electrochemical methods,[15] and photocatalysis have also been used as a green chemistry alternative for the

deuteration of organic compounds.[16] Isotopic ^2H enrichment of labile sites such as NH_n ($n = 1$–3) and OH_n ($n = 1, 2$) groups can be achieved by treating the samples with deuterated solvents, facilitating the NMR analysis of biomacromolecules,[17] though it leads to low yields of deuteration. Here, we present a facile chemical exchange protocol to deuterate labile protons in pharmaceutical compounds by dissolution and crystallization from a ^2H-enriched solvent at different temperatures, yielding up to 90% deuterium substitution. The high degree of H/D exchange enabled the structural elucidation of drug molecules in solid formulations by magic-angle spinning (MAS) NMR spectroscopy.

The multistep approach we propose for site-specific deuteration in small molecules is presented in Fig. 1. The process begins with the dissolution of small molecules in deuterated solvents, in which the labile protons in amine, imide, and hydroxyl groups are exchanged by deuterium, but not the CH_n ($n = 1$–3) sites. The rate of H/D exchange depends on proton
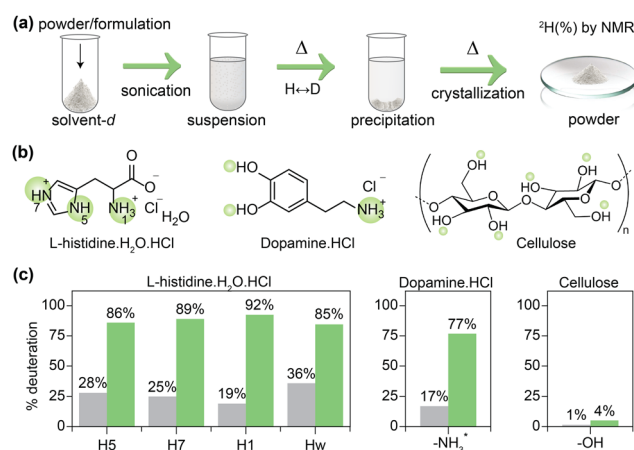
Fig. 1 (a) A schematic of site-selective H–D exchange for small molecules, (b) molecular structures of L-histidine·HCl·H_2O, dopamine·HCl and cellulose, and (c) the degree of deuteration measured by ^1H MAS NMR spectroscopy. Grey and green bars correspond to the deuteration (%) obtained at 295 K and 373 K. *contribution from OH.

[a] *University of Lille, CNRS, Centrale Lille Institut, Univ. Artois, UMR 8181 – UCCS – Unité de Catalyse et Chimie du Solide, F-59000, Lille, France.*
  E-mail: gnm.reddy@univ-lille.fr
[b] *University of Lille, CNRS, INRAE, Centrale Lille, Univ. Artois, FR 2638 – IMEC – Institut Michel-Eugène Chevreul, F-59000, Lille, France*

† Electronic supplementary information (ESI) available: Experimental details and NMR spectral analysis. See DOI: https://doi.org/10.1039/d2cc04585k
‡ Equally contributed to this work.

lability and solubility, as well as the crystallization temperature. The extent of H/D exchange can be assessed by analysing ^1H MAS NMR spectra of the powder before and after deuteration (ESI,† Section 2). For L-histidine·HCl·H$_2$O and dopamine·HCl, degree of deuteration (%) is presented in Fig. 1c (ESI,† Fig. S1) for different sites as a function of temperature. Crystallization from D$_2$O at 295 ($\pm$3) K enables H/D exchange yields of 19% and 17% for the NH$_3$ sites in L-histidine·HCl·H$_2$O, and dopamine·HCl, respectively. Crystallization at 373 ($\pm$3) K yields a more facile exchange, resulting in 92% and 77% of deuteration for the same sites. A high degree of deuteration can be achieved in a single cycle where the temperature is not a concern. However, multiple cycles of deuteration and recrystallization may be required for the biological systems at relatively low temperatures ($<$290 K). In contrast, cellulose is poorly soluble in water and exhibits low affinity towards H/D exchange (Fig. 1c, and ESI† Fig. S2) even at high temperatures. It is also expected to be the case for saturated fatty acids, polymer micelles, and glidants used in pharmaceutical formulations. Therefore, the presented approach can be used to isotopically enrich labile hydrogen atoms in the APIs without significantly deuterating excipients. Below, we illustrate how this method can be used to selectively detect histidine and dopamine in solid formulations.

Although deuterated compounds have been widely investigated in the context of medicinal chemistry,[4] the molecular-level understanding of amorphous solid dispersions has been exceedingly challenging to obtain due to the compositional and structural heterogeneities associated with APIs and excipients. Solid-state NMR spectroscopy has been used to elucidate local structures, packing interactions, and (pseudo)polymorphism in pharmaceutical compounds.[18,19] Specifically, 2D experiments such as ^1H–X (X = ^1H, ^{13}C, $^{14/15}N$, ^{19}F, and ^{35}Cl) enabled the local structures and interactions in neat APIs and solid formulations to be elucidated.[19–24] One notable example is the use of 2D ^1H–^{14}N and ^{14}N-filtered ^1H–^1H correlation experiments coupled with spin-diffusion process for detecting APIs in solid formulations.[21,23] The proposed 2D ^1H–^2H iCOSY experiment operates in a manner akin to what is observed in ^1H–^{14}N correlation experiments, nonetheless the H/D exchange of –NH$_n$ and –OH$_n$ manifests more ^2H sites to be excited and resolved in APIs.

Fig. 2a compares ^1H MAS spectra of neat and partially deuterated histidine, showing differences in the peak intensities for NH(5) and NH(7), NH$_3$(1), and water (w) protons. In the ^2H MAS NMR spectrum of the latter compound (Fig. 2b), strong intensity peaks corresponding to ND$_3$ and water-d peaks are observed, and weak intensity broad peaks are appeared for D5 and D7 sites. For small molecules, sensitivity and resolution aspects of ^2H MAS NMR have previously been discussed.[25–28] Molecular motions reduce the quadrupolar interactions, allowing narrow ^2H peaks to be detected.[25,26,29,30] Resolution can be substantially improved by MAS in conjunction with high magnetic fields (ESI,† Fig. S3 and S4), enabling the isotropic ^2H chemical shifts as well as quadrupolar couplings to be measured and compared for different sites (ESI,† Fig. S5 and Table S1).

A simple route to acquire 2D ^1H–^2H iCOSY spectra is to use a heteronuclear multiple-quantum coherence (HMQC) pulse
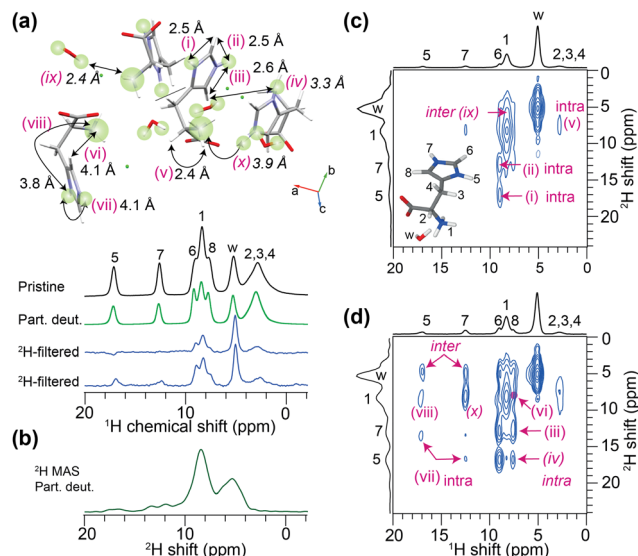

Fig. 2 (a) 1D ^1H MAS spectra of L-histidine·HCl·H$_2$O: pristine (black) and deuterated (green) with a ^2H-filter using different recoupling times (blue), along with (b) a ^2H MAS spectrum of the same compound. 2D ^1H–^2H iCOSY spectra acquired with (c) short (133.3 μs) and (d) long (200 μs) recoupling times. ^1H–^2H distances are depicted in inset (a).§¶ All spectra were acquired at 18.8 T (^1H = 800.1 MHz, 60 kHz MAS).

sequence[31,32] (ESI,† Fig. S1), in which the recoupling delay (τ_{rcpl}) can be adjusted to detect 2D peaks corresponding to ^1H–^2H sites separated by short ($<$3 Å) and mid-range (3–5 Å) distances. The blue spectra (Fig. 2a) illustrate that, a priori, by adjusting the ^1H–^2H recoupling time, all ^1H peaks can be detected. By comparison, 2D iCOSY spectra acquired with 133.3 μs and 200 μs (Fig. 2c and d) recoupling times display peaks corresponding to short ($<$3 Å) and mid-range ($>$3 Å) ^1H–^2H proximities, as depicted in the inset (Fig. 2a).[33] In Fig. 2c, 2D peaks associated with D5–H6, D7–H6/H8, ND$_3$–CH$_2$, CH$_2$–D$_2$O, and ND$_3$–D$_2$O are detected.§ In Fig. 2d, detection of the 2D peaks corresponding to through-space D5–H8 (iv) and ND$_3$–H8 (vi) proximities with ^1H–^2H distances $>$4 Å is noteworthy.§ Meanwhile, one has to take into account that the ^2H isotope substitution may lead to shorter bond distances.[6]¶

Next, we studied a solid formulation consisting of L-histidine·HCl·H$_2$O and cellulose (20/80 wt%) using the 2D ^1H–^2H iCOSY approach. For this blend, 1D ^1H (before and after deuteration), $^1H\{^2H\}$ and ^2H MAS spectra are shown in the ESI† (Fig. S6), in which the ^2H-filter suppresses the cellulose signals enabling the histidine peaks to be resolved. Fig. 3 presents 2D iCOSY spectra, whereby the spectrum acquired with a short recoupling time (100 μs, Fig. 3a) showed peaks associated with ND$_3$/NH$_3$ and H$_2$O/D$_2$O, whereas a long recoupling time (200 μs, Fig. 3b) allowed 2D peaks corresponding to the ND$_3$-water, water-H5/H7/H8, water-CH$_2$ and ND$_3$–H5 proximities to be detected. In addition, weak intensity peaks associated with cellulose (cyan box) are observed. Key learning from this analysis is that the local structures of partially deuterated molecules in complex solid formulations can be resolved and identified.
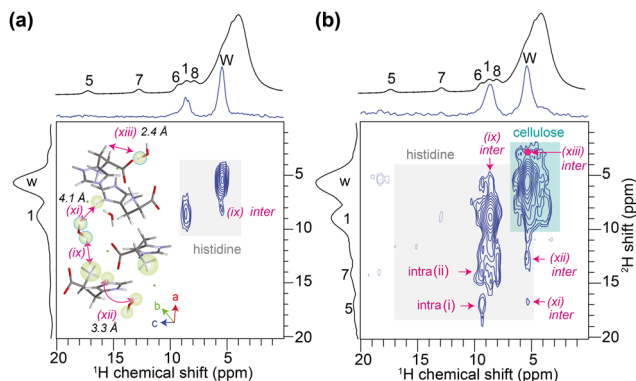
Fig. 3 2D ^{1}H–^{2}H iCOSY spectra of partially deuterated histidine-cellulose (20/80 wt%) blend acquired with (a) 99.9 μs and (b) 199.8 μs of mixing time, plotted with the projections. 1D ^{1}H MAS spectra (black) are presented in the top.

The sensitivity and resolution capabilities of high-field ^{2}H NMR for characterising drug formulations are further examined by analysing dopamine(DOPA)-cellulose blends, with different DOPA concentrations in the 5–30 wt% range. DOPA and its analogue levodopa (L-DOPA) have been widely investigated in the context of Parkinson's disease and related disorders.[34] Fig. 4 compares ssNMR spectra of DOPA and DOPA-cellulose blends, in which neat DOPA (Fig. 4a) displays a broad peak at ∼7.6 ppm due to an overlapped contribution from NH$_3$ and aromatic protons, and partially resolved peaks at 2–4 ppm and 4–6 ppm are due to the CH$_2$ (2, 2', 3 and 3') moieties. While all ^{1}H peaks are observed in the ^{1}H MAS spectra of pristine (black) and partially deuterated DOPA (green), the

^{1}H{^{2}H} MAS spectrum of the latter (blue) yields selective detection of the peak at ∼7.6 ppm (NH$_3$/ND$_3$ and OH/OD). Consequently, ^{2}H MAS spectrum (green, bottom) displays a peak at ∼7.6 ppm, facilitating the analysis of chemical shifts and quadrupolar parameters of ND$_3$ and OD (ESI,† Fig. S7, S8 and Table S2). For the same compound, the 2D ^{1}H–^{2}H iCOSY spectrum (Fig. 4b, and ESI† Fig. S9) shows a strong peak originating from NH$_3$/ND$_3$ and a weak intensity peak corresponding to ND$_3$/CH$_2$ proximities.[33] In comparison, DOPA-cellulose blends exhibit severely overlapped ^{1}H MAS NMR spectra (Fig. 4c) with peaks originating from cellulose. Notably, detection of the ^{1}H peak at 7.8 ppm for 5 wt% DOPA (∼100 μg, for which ∼75% NH$_3$ sites are deuterated) illustrates the resolving power of high field ssNMR (28.2 T) for the analysis of a complex solid form. However, structurally disordered arrangements of the excipients give rise to chemical shift distributions (2–7 ppm) that cannot be averaged out even under fast MAS at high fields. Since excipients do not exhibit a tendency towards H/D exchange, their broad spectral features can be easily eliminated by acquiring ^{2}H NMR spectra (Fig. 4c, bottom). High-resolution ^{2}H NMR spectra of DOPA in the blend can be detected in under a minute (∼10 seconds with a signal/noise of ∼20). Likewise, we acquired 1D ^{1}H and ^{1}H{^{2}H} MAS (Fig. 4d, blue) and 2D ^{1}H–^{2}H iCOSY spectra to analyse the local structure of DOPA in the blend. In the 2D iCOSY spectrum (Fig. 4d, bottom), peaks correlating ^{2}H (∼7.6 ppm) and ^{1}H (5.9 and 3.4 ppm) chemical shifts are due to intramolecular proximity between the NH$_3$ and CH$_2$ groups (distances are shown in ESI,† Fig. S10). By comparison, low intensity 2D peaks between the ^{2}H (∼5.5 ppm) and signals ^{1}H (5.5–3.0 ppm) are expected to arise from the cellulose, and the 2D
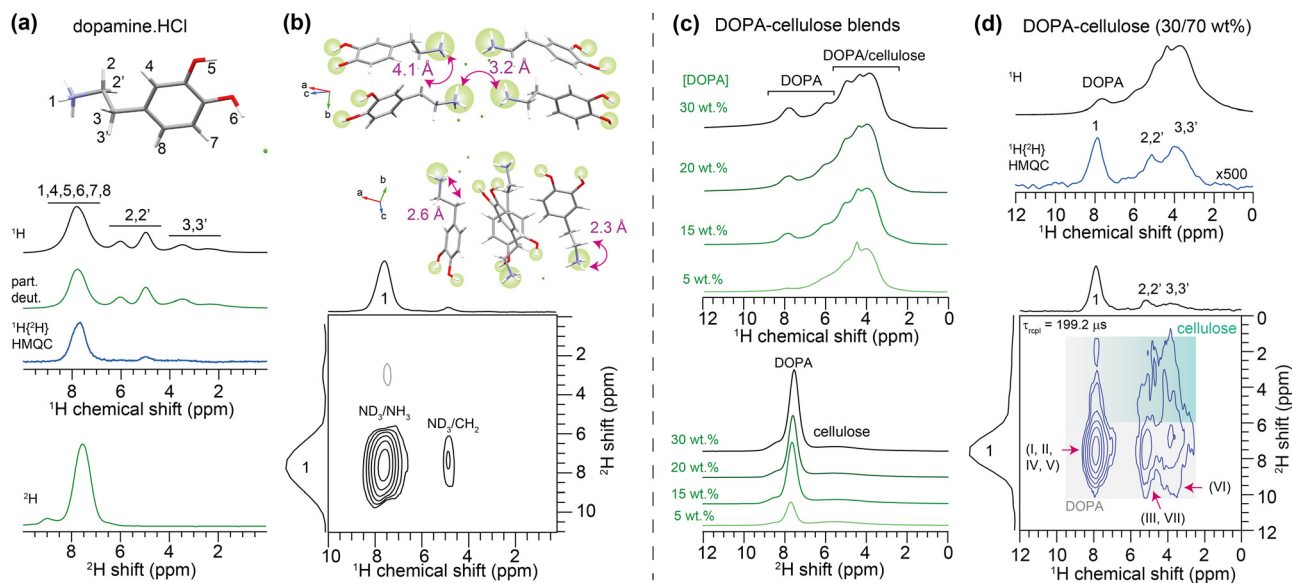

Fig. 4 Structure elucidation of DOPA and DOPA-cellulose blends. (a) top: 1D ^{1}H MAS spectra of pristine (black) and partially deuterated (green) DOPA and with a ^{2}H-filter (blue) and ^{2}H NMR spectrum (bottom) of the same sample acquired at 18.8 T (^{1}H = 800.1 MHz, 60 kHz MAS). (b) A 2D ^{1}H–^{2}H iCOSY spectrum of DOPA acquired at 18.8 T with τ_{RCPL} = 199.8 μs together with the crystal structure depicting the interatomic distances. (c) 1D ^{1}H MAS spectra (top) of DOPA-cellulose blends with different concentrations of DOPA as indicated, and ^{2}H NMR spectra (bottom) of the same compounds acquired at 28.2 T (^{1}H = 1200.5 MHz, 60 kHz MAS). (d) A 1D ^{1}H MAS spectrum of pristine (black) and a ^{2}H-filtered (blue) spectrum of the DOPA-cellulose blend along with a 2D iCOSY spectrum acquired with the same conditions as in (b). Distances corresponding to (I–VII) are shown in ESI,† Fig. S10.

peak between ^{2}H ($\sim$5.5 ppm) and ^{1}H ($\sim$7.8 ppm) is likely to indicate the through-space ND$_3$–CH$_2$ proximities (DOPA) as well as the DOPA-cellulose proximities.

In this communication we present a facile route to deuterate the labile protons in pharmaceutical compounds, while excipients do not exhibit this trend due to the poor solubility in water. Stimulated by the ^{2}H enrichment, this study presents a 2D ^{1}H–^{2}H iCOSY technique for detecting APIs in solid formulations. Compared to conventional 2D ^{1}H–^{14}N HMQC, the ^{1}H–^{2}H iCOSY approach benefits from: (i) relatively large ^{1}H–^{2}H dipolar couplings than the ^{1}H–^{14}N dipolar couplings despite the low natural abundance of ^{2}H (0.015%), (ii) smaller quadrupolar interactions in ^{2}H than ^{14}N sites, and (ii) there are more ^{2}H{^{1}H} sites that can be labelled in APIs than the naturally occurring ^{14}N{^{1}H} sites, which is an added advantage for the structure elucidation. Cross-polarization (CP) and spin-diffusion techniques provide further sensitivity enhancements in 2D ^{1}H–^{2}H iCOSY spectra.[33,35] Therefore, the iCOSY approach is likely to see a promising future for solid-state characterization.

Conflicts of interest

There are no conflicts to declare.

Notes and references

§ Interatomic distances are measured from periodic DFT geometry optimized crystal structure (ESI,† Experimental section).
¶ C–D bond is shorter by 0.5 picometers compared to the C–H bond, and a shortening is expected for the N–D bond distances.

1 S. Kopf, F. Bourriquen, W. Li, H. Neumann, K. Junge and M. Beller, *Chem. Rev.*, 2022, **122**, 6634–6718.
2 J. Atzrodt, V. Derdau, W. J. Kerr and M. Reid, *Angew. Chem., Int. Ed.*, 2018, **57**, 1758–1784.
3 B. Czeskis, C. S. Elmore, A. Haight, D. Hesk, B. D. Maxwell, S. A. Miller, T. Raglione, K. Schildknegt, J. F. Traverse and P. Wang, *J. Labelled Compd. Radiopharm.*, 2019, **62**, 690–694.
4 S. H. DeWitt and B. E. Maryanoff, *Biochemistry*, 2018, **57**, 472–473.
5 T. G. Gant, *J. Med. Chem.*, 2014, **57**, 3595–3611.
6 T. Pirali, M. Serafini, S. Cargnin and A. A. Genazzani, *J. Med. Chem.*, 2019, **62**, 5276–5297.
7 R. Agarwal, M. D. Smith and J. C. Smith, *J. Chem. Theory Comput.*, 2020, **16**, 2529–2540.
8 S. Hanashima, Y. Ibata, H. Watanabe, T. Yasuda, H. Tsuchikawa and M. Murata, *Org. Biomol. Chem.*, 2019, **17**, 8601–8610.
9 R. Pony Yu, D. Hesk, N. Rivera, I. Pelczer and P. J. Chirik, *Nature*, 2016, **529**, 195–199.
10 G. Prakash, N. Paul, G. A. Oliver, D. B. Werz and D. Maiti, *Chem. Soc. Rev.*, 2022, **51**, 3123–3163.
11 T. R. Puleo, A. J. Strong and J. S. Bandar, *J. Am. Chem. Soc.*, 2019, **141**, 1467–1472.
12 Z. P. Vang, A. Reyes, R. E. Sonstrom, M. S. Holdren, S. E. Sloane, I. Y. Alansari, J. L. Neill, B. H. Pate and J. R. Clark, *J. Am. Chem. Soc.*, 2021, **143**, 7707–7718.
13 W. Li, J. Rabeah, F. Bourriquen, D. Yang, C. Kreyenschulte, N. Rockstroh, H. Lund, S. Bartling, A. E. Surkus, K. Junge, A. Brückner, A. Lei and M. Beller, *Nat. Chem.*, 2022, **14**, 334–341.
14 T. J. Doyon and A. R. Buller, *J. Am. Chem. Soc.*, 2022, **144**, 7327–7336.
15 P. L. Norcott, *Chem. Commun.*, 2022, **58**, 2944–2953.
16 P. Ranjan, S. Pillitteri, E. V. Van Der Eycken and U. K. Sharma, *Green Chem.*, 2020, **22**, 7725–7736.
17 B. Reif, *J. Magn. Reson.*, 2012, **216**, 1–12.
18 A. J. Rossini, C. M. Widdifield, A. Zagdoun, M. Lelli, M. Schwarzwälder, C. Copéret, A. Lesage and L. Emsley, *J. Am. Chem. Soc.*, 2014, **136**, 2324–2334.
19 M. Li, W. Xu and Y. Su, *TrAC, Trends Anal. Chem.*, 2021, **135**, 116152.
20 A. S. Tatton, T. N. Pham, F. G. Vogt, D. Iuga, A. J. Edwards and S. P. Brown, *Mol. Pharmaceutics*, 2013, **10**, 999–1007.
21 M. Grüne, R. Luxenhofer, D. Iuga, S. P. Brown and A. C. Pöppler, *J. Mater. Chem. B*, 2020, **8**, 6827–6836.
22 X. Lu, D. Skomski, K. C. Thompson, M. J. McNevin, W. Xu and Y. Su, *Anal. Chem.*, 2019, **91**, 6217–6224.
23 Y. L. Hong, G. N. M. Reddy and Y. Nishiyama, *Solid State Nucl. Magn. Reson.*, 2020, **106**, 101651.
24 C. M. Quinn, R. Zadorozhnyi, J. Struppe, I. V. Sergeyev, A. M. Gronenborn and T. Polenova, *Anal. Chem.*, 2021, **93**, 13029–13037.
25 T. Mizuno, T. Nemoto, M. Tansho, T. Shimizu, H. Ishii and K. Takegoshi, *J. Am. Chem. Soc.*, 2006, **128**, 9683–9686.
26 A. E. Aliev, S. E. Mann, D. Iuga, C. E. Hughes and K. D. M. Harris, *J. Phys. Chem. A*, 2011, **115**, 5568–5578.
27 M. Schulz-Dobrick and I. Schnell, *Cent. Eur. J. Chem.*, 2005, **3**, 245–251.
28 A. J. Rossini, J. Schlagnitweit, A. Lesage and L. Emsley, *J. Magn. Reson.*, 2015, **259**, 192–198.
29 D. J. Kubicki, D. Prochowicz, A. Hofstetter, P. Péchy, S. M. Zakeeruddin, M. Grätzel and L. Emsley, *J. Am. Chem. Soc.*, 2017, **139**, 10055–10061.
30 P. Raval, R. M. Kennard, E. S. Vasileiadou, C. J. Dahlman, I. Spanopoulos, M. L. Chabinyc, M. Kanatzidis and G. N. M. Reddy, *ACS Energy Lett.*, 2022, **7**, 1534–1543.
31 S. Cavadini, S. Antonijevic, A. Lupulescu and G. Bodenhausen, *J. Magn. Reson.*, 2006, **182**, 168–172.
32 Z. Gan, J. P. Amoureux and J. Trébosc, *Chem. Phys. Lett.*, 2007, **435**, 163–169.
33 P. Raval, J. Trébosc, T. Pawlak, Y. Nishiyama, S. P. Brown and G. N. M. Reddy, *Solid State Nucl. Magn. Reson.*, 2022, **120**, 101808.
34 F. Schneider, L. Erisson, H. Beygi, M. Bradbury, O. Cohen-Barak, I. D. Grachev, S. Guzy, P. S. Loupe, M. Levi, M. McDonald, J. M. Savola, S. Papapetropoulos, W. G. Tracewell, M. Velinova and O. Spiegelstein, *Br. J. Clin. Pharmacol.*, 2018, **84**, 2422–2432.
35 S. K. Jain, A. B. Nielsen, M. Hiller, L. Handel, M. Ernst, H. Oschkinat, Ü. Akbey and N. C. Nielsen, *Phys. Chem. Chem. Phys.*, 2014, **16**, 2827–2830.